THESIS

STATIONARY WAVE TRAINS IN STEEP CHANNELS: EXPERIMENTAL HYDRAULICS AND VELOCITY ESTIMATION

Submitted by

Brooke Pennington

Department of Civil & Environmental Engineering

In partial fulfillment of requirements

For the Degree of Master of Science

Colorado State University

Fort Collins, Colorado

Spring 2026

Master's Committee:

Advisor: Daniel White

Peter Nelson
Ellen Wohl

ABSTRACT

STATIONARY WAVE TRAINS IN STEEP CHANNELS: EXPERIMENTAL HYDRAULICS AND VELOCITY ESTIMATION

Stationary wave trains have been interpreted as indicators of near-critical flow and associated with undular hydraulic jumps (UHJs) in steep rivers. However, the hydraulic conditions under which these waves form, and the extent to which their observable properties reflect flow characteristics, remain incompletely understood. This study investigates stationary wave trains as a hydraulically definable class of surface gravity waves characterized by consistent wavelength across multiple downstream undulations and a mean water surface parallel to the bed slope. Controlled flume experiments were conducted across a range of slopes and discharges to quantify wave geometry, flow depth, and velocity, and to evaluate the applicability of wave-based velocity estimation methods derived from linear wave theory. Stationary wave trains were observed under both subcritical and near-critical flow regimes, with wave nonlinearity increasing systematically with slope. Despite this increase in wave nonlinearity, intermediate-depth dispersion relationships provided the most accurate estimates of mean flow velocity for all slopes tested. These results demonstrate that stationary wave trains are not restricted to classical UHJs and do not require strict critical flow conditions. Instead, they represent organized surface gravity waves that can persist across subcritical to near-critical regimes in steep, rough-bed channels. The findings support the use of wave-based approaches for velocity estimation and provide the hydraulic conditions for interpreting stationary wave trains in natural rivers.

ACKNOWLEDGEMENTS

I would like to sincerely thank my advisor, Danny White, for his guidance, support, and encouragement throughout this research. His mentorship was invaluable during every stage of this research. I am also grateful to the Colorado State University Hydraulics Laboratory for providing the facilities and support needed to conduct the flume experiments, and specifically to Catherine Lambert for her help during the early stages of the experimental setup. I would especially like to thank my parents for their constant encouragement, support, and belief in me throughout my academic journey. I would not be where I am today without their guidance, sacrifices, and constant support. In particular, I want to thank my dad for inspiring my interest in civil engineering and rivers, and for encouraging me to pursue my master's and a career in river engineering. I am also thankful for the friendships I have formed during my time at Colorado State University, which made this experience both meaningful and memorable. Finally, I thank God for the many opportunities and blessings in my life that have made this journey possible.

TABLE OF CONTENTS

LIST OF TABLES

LIST OF FIGURES

LIST OF EQUATIONS

1. INTRODUCTION

Undular free-surface flows occur across a wide range of flow environments and are particularly common in steep-gradient channels where rapid acceleration, bed roughness, bed mobility, and geometric irregularities promote the development of surface waves (Kennedy, 1963; Henderson, 1966; Kieffer, 1985, 1987; Chanson & Montes, 1995; Tinkler, 1997b, 1997a; Grant, 1997; Chanson, 2000; Comiti & Lenzi, 2006; Magirl et al., 2009; Dietterich et al., 2022). In natural rivers, these undulations often appear as spatially organized sequences of standing waves within rapids and high-gradient reaches. These standing wave trains have long been associated with near-critical flow conditions (Kennedy, 1963; Henderson, 1966; Grant, 1997; Tinkler, 1997a; Montes & Chanson, 1998; Chanson, 2000; Magirl et al., 2009).

However, the term standing wave, encompasses a range of free-surface wave responses, including wave fields associated with undular hydraulic jumps (UHJs) as well as persistent wave sequences without a supercritical-to-subcritical transition. In this study, we introduce the term stationary wave trains to distinguish a specific class of coherent, standing surface gravity waves that persist over extended downstream distances while maintaining a mean water surface approximately parallel to the bed slope. The hydraulic conditions that permit the formation and persistence of these stationary wave trains have not been studied. Additionally, it is unclear whether their observable wave characteristics reflect mean flow characteristics.

Flow in open channels is often classified using the Froude number (Fr), which compares inertial forces to gravitational restoring forces,

$$Fr = \frac{U}{\sqrt{gh}} \tag{1}$$

where U is the mean flow velocity, g is gravitational acceleration, and h is the mean flow depth. Physically, Fr represents the ratio of the mean flow velocity to the speed at which small-amplitude shallow-water surface gravity waves propagate. Subcritical flow ($Fr < 1$) permits upstream propagation of surface disturbances and indicates downstream hydraulic control, whereas supercritical flow ($Fr > 1$) permits only downstream propagation (Chow, 1959; Henderson, 1966). The condition $Fr = 1$ defines critical flow and marks the transition between these two regimes (Chow, 1959; Henderson, 1966). The stated physical interpretation of *Fr* as a measure of hydraulic control rests on the shallow-water approximation, in which wave celerity is independent of wavelength and pressure is assumed hydrostatic. In this long-wavelength limit, wave speed is given by $\sqrt{gh}$. Although steep natural rivers may not strictly satisfy these conditions, *Fr* remains the dominant framework for interpreting free-surface flow regime in steep rivers.

Wave celerity (c) is derived from linear wave theory (Airy, 1845; Phillips, 1977; Stokes, 1847) and depends on the ratio of flow depth to wavelength (h/L). Under the shallow-water condition ($h/L < 0.05$), celerity is independent of wavelength and given by $c_s = \sqrt{gh}$ which forms the basis for the physical interpretation of Fr described above. However, when wavelength is not large relative to depth, wave celerity depends on both depth and wavelength according to the full dispersion relation, $c_g = \sqrt{\frac{gL}{2\pi}\tanh\left(2\pi\frac{h}{L}\right)}$. In the deep-water limit ($h/L > 0.5$), celerity depends only on wavelength, $c_d = \sqrt{\frac{gL}{2\pi}}$. White et al. (2026) show that surface waves in open channel flows frequently occur under intermediate-depth conditions, where celerity is not well approximated by either the shallow- or deep-water limits and instead depends on wavelength through the full dispersion relation, c_g. Stationary wave trains observed in steep

rivers may likewise not satisfy the shallow-water condition. However, to our knowledge, no studies have systematically evaluated the depth-wavelength regime under which persistent stationary wave trains occur in steep, rough channels.

Recent studies interpret wave trains in steep rivers as indicators of UHJs and, by extension, as evidence of near-critical flow conditions (Grant, 1997; Legleiter et al., 2025). UHJs represent one well-characterized class of free-surface oscillation in which supercritical flow adjusts to subcritical conditions through a spatially extended train of surface waves rather than through a single abrupt roller (Chanson & Montes, 1995). They form when the approach Fr is slightly greater than unity and the flow's specific energy is close to minimum, producing a smooth rise of the free surface followed by standing wave oscillations downstream of the jump toe (Montes & Chanson, 1998; Chanson, 2009; Castro-Orgaz & Hager, 2017; Hager & Castro-Orgaz, 2019; Hu et al., 2023). Although UHJs may be common in steep rivers, for example at slope breaks, constrictions, or depth transitions, not all free-surface wave trains necessarily satisfy the hydraulic criteria defining a super-subcritical transition, and other forms of persistent surface oscillation may occur under different flow conditions.

Broadly speaking, wave trains in steep rivers have been documented in both natural and experimental settings, often hypothesized to occur under near-critical flow conditions ($Fr \approx 1$) (Grant, 1997; Tinkler, 1997a). Early field observations by Kieffer (1985, 1987) described stable wave trains in Colorado River rapids, noting that while wave amplitude varies with discharge, wave position remains relatively fixed due to bed controls. Previous theoretical and experimental work has linked stationary wave formation to near-critical flow conditions in which mean flow velocity is comparable to the celerity of surface gravity waves (Kennedy, 1963), and steep channels ($0.01 < \text{slope} < 0.03$) commonly exhibit near-critical behavior (Comiti & Lenzi, 2006).

Grant (1997) further proposed that flows in steep channels tend to asymptotically approach critical flow, motivating wave-based approaches that relate observable wave properties to mean flow velocity. Tinkler (1997b) showed that wavelength can provide accurate non-contact estimates of mean flow in steep rock-bed rivers. Subsequent studies (Dietterich et al., 2022; Legleiter et al., 2025) extended these approaches using remote sensing to estimate discharge from channel width and wavelength. White et al. (2026) assessed the sensitivities to assumed Fr, wave dispersion assumptions, and the link between wave celerity and mean velocity in UHJs.

Collectively, these studies describe relationships between wave characteristics and mean flow properties; however, these wave-based approaches have not been evaluated alongside other commonly used methods for estimating flow velocity in steep mountain streams. For example, Yochum et al. (2012) evaluated non-wave-based velocity prediction methods for steep mountain streams, yet direct comparisons between wave-derived approaches and the methods evaluated by Yochum et al. (2012) have not been conducted.

To our knowledge, a rigorous classification framework defining the hydraulic conditions under which different types of wave trains emerge in steep, rough channels has not been systematically developed. To that end, we document, analyze, and define one specific class of free-surface oscillation occurring in steep channels which we term *stationary wave trains.*

Stationary wave trains are defined here as coherent sequences of surface gravity waves with undular morphology that persist over extended downstream distances without measurable wavelength attenuation and exhibit a mean water surface approximately parallel to the bed slope (Figure 1a). We investigated this class of wave feature using controlled laboratory experiments in a fixed rough-bed flume, in which slope and discharge were systematically varied (Figure 1c). Complementary field observations demonstrate that similar wave trains occur in natural rivers,

extending over distances greater than ten channel widths, as documented through recent remote sensing analyses (e.g., Figure 1b; White et al., 2025).

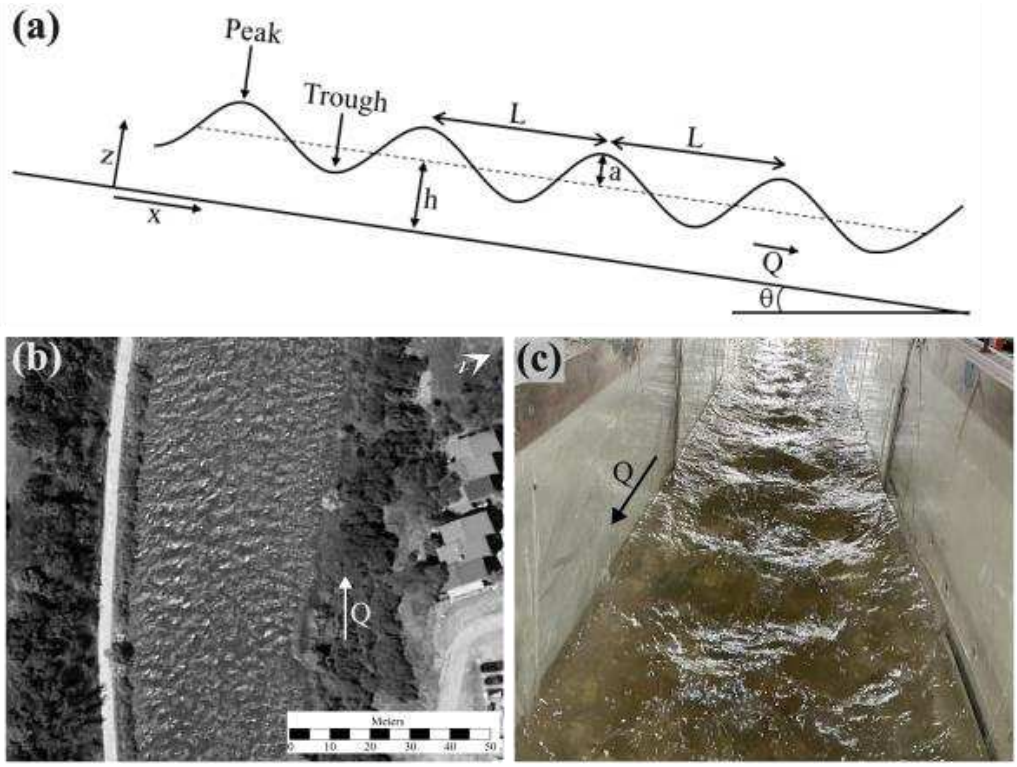

Figure 1. Stationary wave trains in nature and laboratory setting. (a) Stationary wave train graphical schematic. (b) Stationary wave trains observed in the Roaring Fork River, Glenwood Spring, Colorado, identified from satellite imagery. (c) Stationary wave trains generated in the laboratory flume under fixed bed conditions at 1.5% slope, 0.07 m^3/s.

Building on these observations, we quantify the hydraulic conditions under which these waves form and examine the relationship between wave celerity, wavelength, flow depth, mean flow velocity, and mean surface velocity. In doing so, we evaluate whether observable wave characteristics can serve as reliable indicators of the specific energy regime in steep channels. These analyses clarify the physical basis for using surface wave characteristics to interpret hydraulic regime and discharge in steep rivers, where direct measurements are often challenging.

2. METHODS

2.1 Flume Experiment

We conducted a controlled flume experiment at the Colorado State University Hydraulics Laboratory in Fort Collins, Colorado, USA, using an 18.3-m-long, 0.6-m-wide recirculating flume with an adjustable slope (Figure 2). Water was pumped into the flume using a 75-hp pump. We measured the flow rate using a Signet Insertion Magnetic flowmeter and controlled the flow rate using a manual valve to adjust the flow entering the flume. Maximum discharge that the flume could reach was 0.28 m^3/s.

Figure 2. 18.3 m x 0.6 m x 0.6 m recirculating laboratory flume at Colorado State University Hydraulics Lab.

The bed was composed of very coarse gravel (D_{50} = 56 mm) (Figure 3a and Figure 3b). Flow depth was not externally controlled, and no downstream tailwater was imposed. For each slope-discharge combination, we allowed flow to develop naturally over the fixed rough bed. Experiments were conducted at slopes ranging from 1% to 5%, increasing in 0.5% increments. For each slope, discharge was increased in 0.028 m^3/s increments across the tested range. We did not test slopes greater than 5% because natural channels steeper than 5% are typically associated

with step-pool or cascade channel types (Buffington & Montgomery, 2022) which would preclude the formation of stationary wave trains that persist spatially over long downstream distances. For each slope-discharge combination, we visually assessed whether stationary wave trains were formed. We defined stationary wave trains as distinct, continuous sequences of repeating surface peaks and troughs extending longitudinally downstream. Wave trains typically emerged once the flow was fully developed approximately halfway down the flume and extended downstream to the end of the flume. We recorded hydraulic measurements during runs in which stationary waves were visually confirmed and excluded runs where discharges were either too low or high for wave formation. In total, we observed 34 slope-discharge combinations in which stationary wave trains occurred, and we measured their hydraulic characteristics during each of those runs.

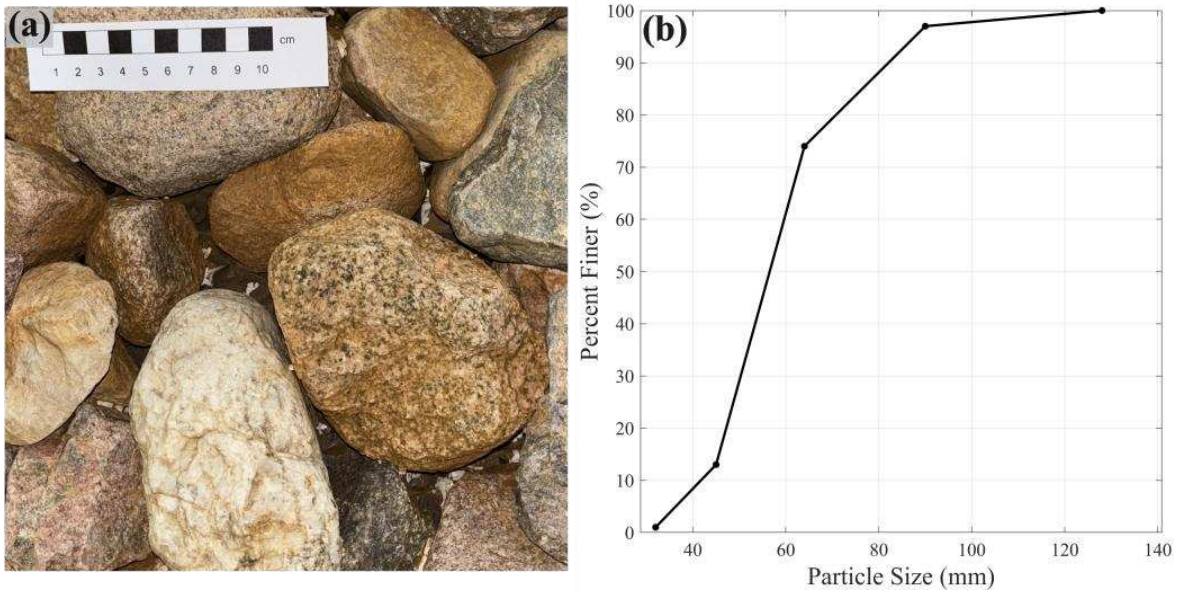

Figure 3. (a) Coarse gravel used to construct the flume fixed bed. (b) Particle size distribution of the flume bed material.

2.2 Wave Geometry Measurements

For each experimental run exhibiting stationary wave trains, we measured wavelength (L), water surface elevation (WSE), and flow depth (h), at wave peaks (denoted by subscript p) and troughs (denoted by subscript t). We measured WSE and h at the channel centerline. To measure wavelength, we visually identified wave peaks and troughs and marked their position on the flume wall and measured peak-to-peak and trough-to-trough distances using a tape measure. Multiple wavelengths were measured during each flume run, and the average wavelength for each run was calculated from these observations. We measured WSE_p and WSE_t by lowering a point gauge referenced to a local coordinate system to the water surface at peaks and troughs. We then lowered the point gauge to the bed to measure bed elevation at locations where persistent peaks and troughs occurred. We calculated h_p and h_t as the difference between the bed elevation and WSE_p and WSE_t. We calculated the average depth for each run as the spatial average of all h_p and h_t measurements. Wave amplitude (a) was calculated from WSE measurements. For each consecutive peak and trough pair, amplitude was computed as $a = \left(\frac{WSE_p - WSE_t}{2}\right)$. Amplitudes from all measured wave pairs within an experiment were averaged to obtain a single representative amplitude value for that run.

Lastly, to characterize bed topography, we scanned the immobile gravel bed over the section of the flume where stationary waves formed using the LiDAR sensor on an iPad. The scan was conducted under dry conditions to document bed morphology independent of the water surface. We used this survey to verify that the bed was approximately planar and did not contain periodic topographic features that could impose forced oscillations on the flow. During the flume runs, we did not observe any mobilization of bed material, and no restructuring of the bed morphology occurred that could impose forced oscillations (i.e., dunes or antidunes).

A separate LiDAR scan was conducted during flow conditions to capture the visual geometry of the stationary wave train. Figure 4 shows the water surface scan of the stationary wave train over the immobile gravel bed.

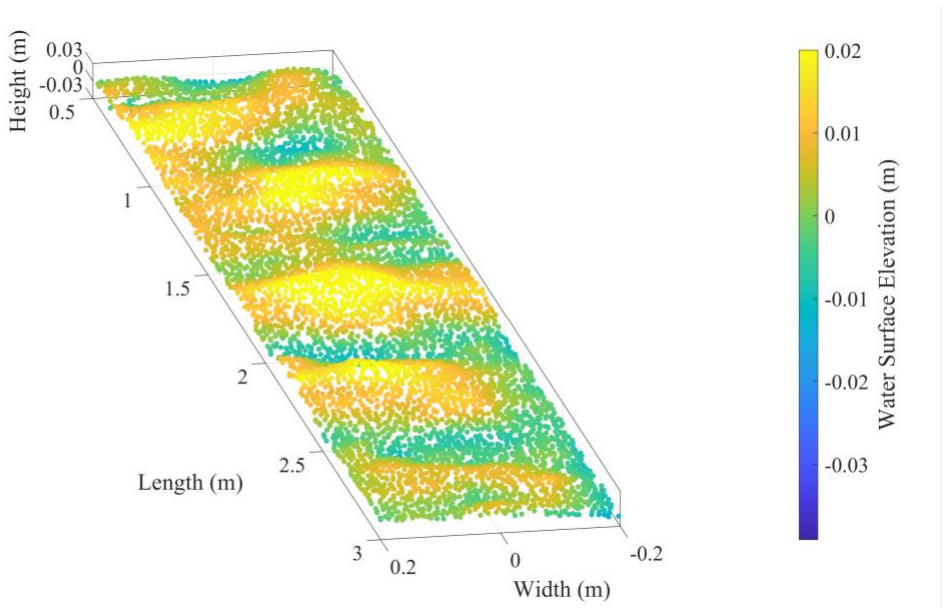

Figure 4. iPad LiDAR scan of a stationary wave train generated in the laboratory flume over nonmobile rough bed (1.5% slope, 0.07 m^3/s). The scan highlights the spatial pattern of wave peaks and troughs along the flume length where 0 is the mean WSE.

The periodic undulations visible along the flume length reflect the spatially repeating peaks and troughs of the stationary waves. The scan was obtained using the integrated LiDAR sensor in an Apple iPad Pro (M4), which operates as a near-infrared time-of-flight system (~940 nm) that estimates distance from the travel time of emitted pulses. At the short measurement distances used in these experiments, a portion of the emitted signal reflects from the water surface rather than being absorbed in the water column, allowing the device to capture the instantaneous water surface geometry. Although the resulting point cloud clearly captures the presence and spatial pattern of the stationary waves, the measurements were not collected within the flume's local

coordinate reference system, and the accuracy of the handheld sensor is insufficient to reliably quantify wave amplitude or wavelength. Accordingly, the LiDAR data are used here only for qualitative visualization of the wave field rather than for quantitative hydraulic measurements.

2.3 Hydraulic Parameters Associated with Stationary Wave Trains

We calculated the hydraulic parameters for each run to identify the range of flow conditions under which stationary wave trains occurred. In each run, we assumed conservation of mass and uniform velocity and depth across the width of the flume. Although the wave pattern near the wall deviated slightly from that at the channel centerline, where WSE measurements were taken, we consider these deviations small, and centerline measurements provide a reasonable representation of the bulk hydraulic conditions used to compute the following hydraulic parameters. The mean flow velocity for each run was calculated using $U = q/h$, where q is unit discharge. Using the unit discharge, channel width (B), mean grain size (D_{50}), mean depth, wavelength, and mean flow velocity, we computed multiple hydraulic parameters to characterize flow regime, roughness influence, and wave behavior of stationary wave trains. The Froude number (Equation 1) indicates the flow regime; The Reynolds number, $Re = UR/\nu$, where R is hydraulic radius, and ν is kinematic viscosity, characterizes fluid flow behavior and provides a general indication of the turbulence flow regime; Relative submergence, h/D_{50}, indicating the degree to which the flow depth exceeds the roughness scale of the bed, helping to assess how bed roughness interacts with the wave field; Shields stress, $\tau_* = \frac{\tau}{(\rho_s - \rho)\, g\, D_{50}}$, where τ is bed shear stress, $\rho_s \; and \; \rho$ are sediment and water density, quantifies the potential for sediment motion and confirms that stationary wave trains form over an immobile bed; Width-to-depth ratio, B/h, describes lateral confinement of the flow, which can influence the stability and coherence, while relative depth, h/L, provides a measure of whether the waves are shallow,

intermediate, or deep-water regimes, affecting wave dispersion behavior; Wave nonlinearity, $\varepsilon = a/h$, describes the degree of linearity of the waves indicates whether linear wave theory is appropriate for interpreting the observed wave characteristics. Table 1 summarizes the experimental conditions of the flume experiments.

Table 1. Summary of experimental conditions for the flume experiments.

Slope (%)	Flow Rate (m^3/s)	Average Froude Number	Average Reynolds Number
1.0	0.028–0.099	0.56	6.93×10^4
1.5	0.057–0.099	0.76	8.72×10^4
2.0	0.028–0.085	0.73	6.77×10^4
2.5	0.028–0.071	0.79	6.13×10^4
3.0	0.042–0.071	0.87	6.94×10^4
3.5	0.042–0.071	1.04	7.08×10^4
4.0	0.042–0.071	0.90	6.96×10^4
4.5	0.028–0.057	0.93	5.51×10^4
5.0	0.028–0.057	0.93	5.54×10^4

2.4 Surface Velocity and Celerity

To measure surface velocity, we flew a drone equipped with a Hasselblad L1D-20c camera featuring a 1-inch 20-megapixel sensor, a 28-mm equivalent lens with adjustable f/2.8–

f/11 aperture, and 4K video resolution above the flume. The stationary camera was oriented nadir towards the water surface at approximately 3 meters above the flow. We seeded the flow surface with lightweight paper tracer particles to visualize surface motion. We processed the recorded video with Large Scale Particle Image Velocimetry (LSPIV) using Fudaa-LSPIV software (LeCoz et al., 2014) and all images were stabilized prior to analysis. Because the camera was positioned and lens distortion was negligible, we scaled the imagery using known flume dimensions. We then superimposed a rectangular computational grid spanning the active flow region. The grid consisting of 16 columns and 25 rows of analysis points distributed across the flume's width and the region containing stationary waves trains. At each grid point, surface velocity was computed by tracking the displacement of tracer particles between sequential image frames and divided by the time interval between frames. Surface velocity at centerline nodes (column 8 and 9) were averaged to determine a representative surface velocity for each run.

To evaluate wave-based velocity estimation, we calculated wave celerity using linear wave dispersion relationships corresponding to shallow-water (c_s), intermediate-depth (c_g), and deep-water (c_d) conditions. Because wave celerity depends on relative depth of flow, we calculated h/L for each experimental run to classify observed waves as shallow, intermediate, or deep-water. This classification is important because shallow-water waves are non-dispersive and independent of wavelength, whereas intermediate- and deep-water waves are dispersive and depend on both flow depth and wavelength. For each run, the average measured wavelength and mean depth were used to compute predicted celerity's from each dispersion formulation. Predicted velocities derived from wave celerity were compared to the measured mean and surface velocities in the flume experiments. In addition, we used published non-wave-based empirical velocity equations for steep mountain streams (Yochum et al., 2012) to compare wave-

based and non-wave-based velocity prediction approaches under stationary wave conditions. Performance of the velocity prediction method was quantified using the coefficient of determination, and predictive performance was evaluated using the root mean square error (RMSE):

$$RMSE = \sqrt{\frac{\sum(predicted - measured)^2}{N}} \quad (2)$$

The statical analysis for each velocity and celerity plot was used to quantify the relative performance of the velocity prediction methods (Appendix A).

2.5 Field Observation

On the Cache la Poudre River, Colorado, USA we assessed stationary wave trains in natural steep rivers using remotely sensed imagery and high-resolution topographic data (White et al., 2025). We identified stationary wave trains using Google Earth remote sensing imagery by recognizing repeating linear features alternating between light and dark strips, with lighter pixels corresponded to surfaces reflecting the sunlight. We measured the distance between points perpendicular to the linear features representing the wavelength (e.g., light-to-light or dark-to-dark) moving downstream, perpendicular to linear wave features. We determined the reach-average elevation by extracting the elevation at each point along the stationary wave train from a LiDAR derived DEM. Despite inherent uncertainty in elevation measurements, reach-average slope was determined by fitting a linear trend line to the DEM data.

3. RESULTS

3.1 Conditions of Stationary Wave Trains

To document the conditions under which stationary wave trains form, we evaluated the average wavelength, flow depth, wave nonlinearity, mean velocity, and surface velocity for each experimental run as a function of channel slope and discharge (Table 2). Stationary wave trains were not observed at a slope of 0.5% for any tested discharge. In contrast, stationary waves were consistently observed for all tested slopes between 1% and 5%. In the experiments, stationary wave trains developed over approximately half the flume length, initiating near mid-flume and extending downstream as fully developed, persistent stationary wave patterns.

Table 2. Summary of stationary wave characteristics observed in the flume experiments for each slope and discharge range.

Slope (%)	**Discharge (cms)**	**Average Wavelength (cm)**	**Average Depth (cm)**	**Wave Nonlinearity $\boldsymbol{\varepsilon = a/h}$**	**Average Velocity $\boldsymbol{U = q/h}$ (m/s)**	**Average Surface Velocity (m/s)**
1	0.028–0.099	33–61	9.7–20	0.028–0.115	0.50–0.82	0.52–0.86
1.5	0.057–0.099	52–76	12.2–17.3	0.048–0.177	0.77–1.0	0.93–1.13
2	0.028–0.085	41–74	8.6–13.7	0.055–0.144	0.57–1.03	0.75–1.21
2.5	0.028–0.071	41–69	8.4–11.4	0.081–0.161	0.56–1.04	0.82–1.19
3	0.042–0.071	53–69	10.2–10.9	0.101–0.122	0.68–1.09	0.90–1.26
3.5	0.042–0.071	55–64	8.1–11.2	0.105–0.144	0.85–1.09	0.84–1.20
4	0.042–0.071	61–69	8.9–11.7	0.127–0.150	0.80–1.0	0.79–1.23
4.5	0.028–0.057	38–69	6.9–10.4	0.141–0.203	0.71–0.92	0.79–1.13

5	0.028–0.057	38-66	6.1–10.4	0.160-0.202	0.78-0.91	0.70–1.13

These stationary wave trains formed over a nonmobile gravel bed, and the bed material did not exhibit periodic undulation that could have imposed free-surface undulations (i.e. antidunes, dunes, ripples). A plan view of the flume LiDAR scan (Figure 5a) shows small variations in bed elevation around the mean bed height, while the longitudinal profile along the flume centerline (Figure 5b), where depth measurements were taken, shows small rock height differences in the bed. These bed elevation patterns do not correspond to the locations or spacing of observed stationary wave train peaks and troughs.

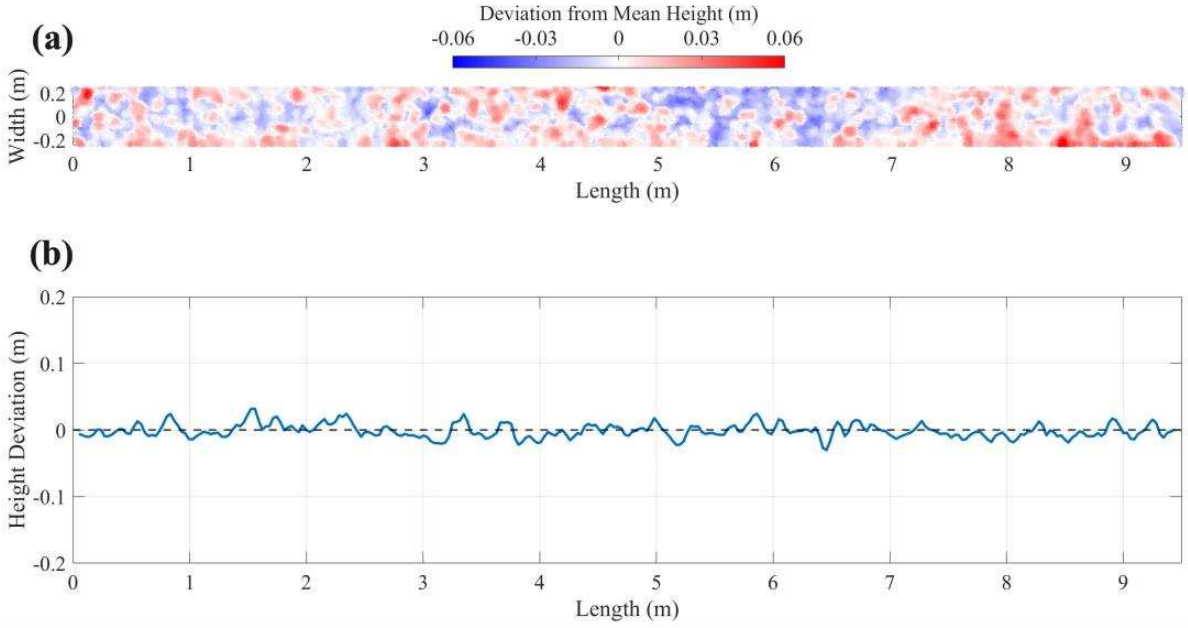

Figure 5. LiDAR scan of the nonmobile flume bed over the section where stationary wave trains were observed. (a) Plan view of bed elevation relative to the mean bed height. (b) Longitudinal bed elevation profile along the flume centerline. Upstream (left), downstream (right).

The hydraulic and geometric conditions associated with stationary wave formation are summarized in Figure 6, which presents occurrence envelopes for relative submergence, Shields

stress, Froude number, width-to-depth ratio, and relative depth as functions of channel slope. Relative submergence decreases systematically with increasing slope (Figure 6a), indicating that stationary wave trains form in progressively shallower flows relative to bed roughness at steeper slopes. Across all runs exhibiting persistent stationary wave trains, relative submergence remains low (1-3.5), indicating progressively lower relative submergence at steeper slopes. At lower slopes (≤ ~2.5%), relative submergence spans a broader range, whereas at steeper slopes the range narrows and shifts toward lower values. Shields stress increases continuously with slope (Figure 6b), reflecting increasing bed shear stress with increasing slope and discharge. All observations fall within a narrow envelope of moderate Shields stress. Although the bed remained immobile in all experiments, the increasing Shields stress indicates progressively greater proximity to incipient sediment motion. Mean Froude number also increases with slope (Figure 6c). Stationary wave trains are observed across subcritical to near-critical flow conditions, with Froude numbers approaching unity at steeper slopes. At lower slopes, flows remain predominantly subcritical, whereas at slopes greater than ~ 3%, Froude numbers for all discharges cluster near-critical or weakly supercritical values. Geometric scaling relationships further characterize the flow conditions associated with stationary wave trains. The width-to-depth ratio increases with slope (Figure 6d), indicating that stationary waves at steeper slopes occur in relatively wider and/or shallower flow configurations. Relative flow depth decreases systematically with increasing slope (Figure 6e), indicating that wavelength increases more rapidly than flow depth as slope increases.

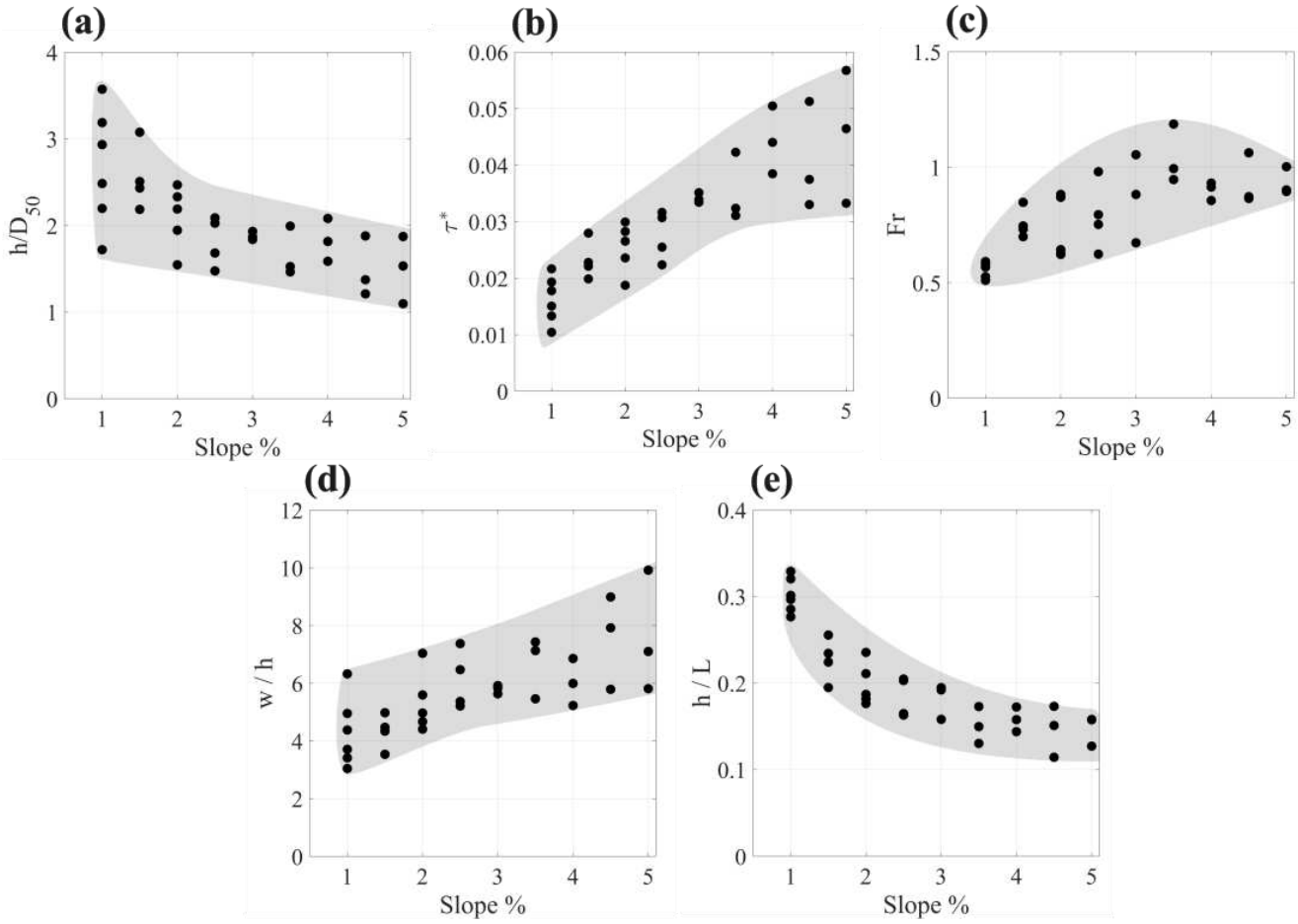

Figure 6. Hydraulic and geometric conditions associated with stationary wave trains across all flume experiments, shown as a function of channel slope: (a) relative submergence (h/D_{50}) , (b) Shields stress (τ_*), (c) mean Froude number (Fr), (d) width-to-depth ratio (w/h), and (e) relative depth (h/L).

Wave nonlinearity increases consistently with slope, showing that stationary wave trains become progressively more nonlinear under steeper flow conditions (Figure 7). At lower slopes and discharges, ε values cluster more within a linear regime, whereas at the steepest slopes, a substantial fraction of observations approach a weakly nonlinear regime.

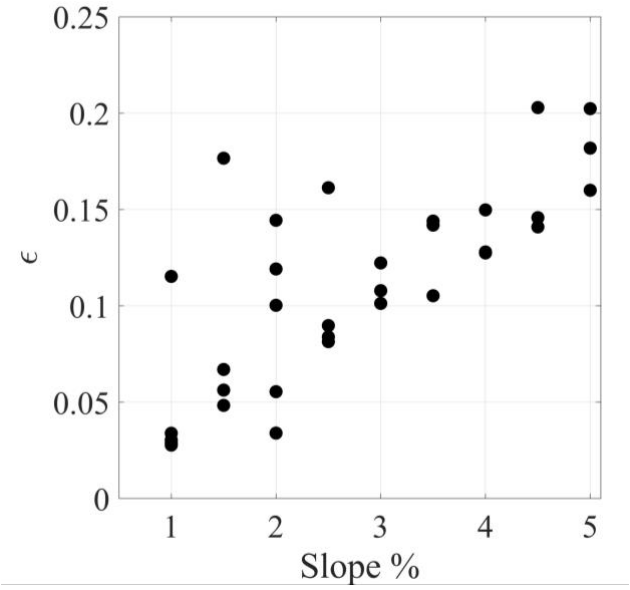

Figure 7. Variation in wave nonlinearity, expressed as ε = a/h, as a function of channel slope for all stationary wave trains observed in all flume experiments.

3.2 Velocity Estimation

For all slope-discharge combinations that produced stationary waves trains in the flume experiments, we observed that the waves fell within the intermediate-depth regime based on the relative depth classification. Figure 8 shows the distribution of observed wave regimes, confirming that all stationary waves were intermediate depth. This finding indicates that the intermediate-depth dispersion relation, c_g, should theoretically provide accurate estimates of wave celerity relative to mean flow velocity for these stationary wave trains.

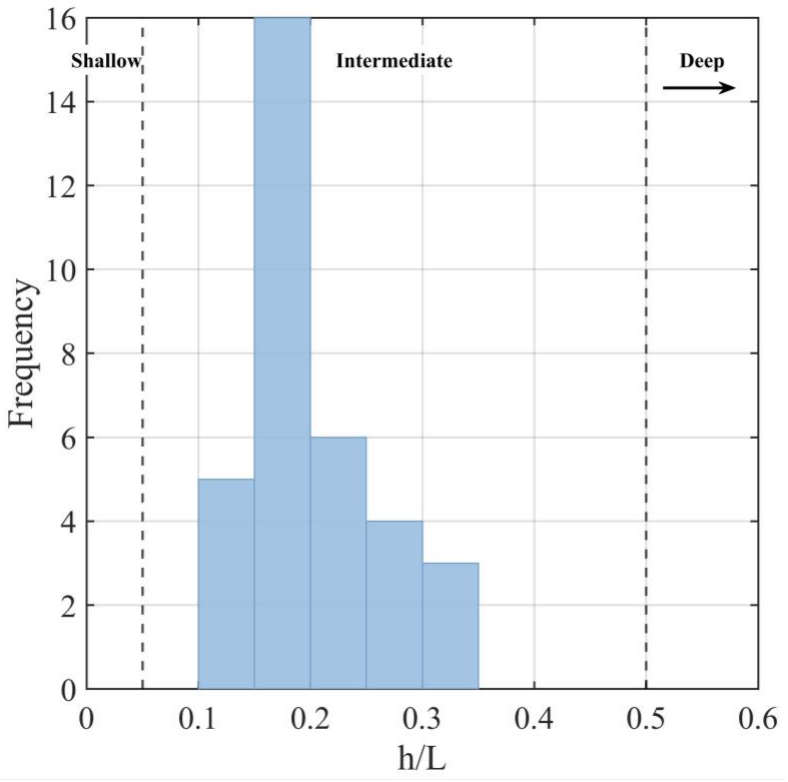

Figure 8. Relative depth (h/L) classification of stationary waves in flume experiments.

We compared measured mean velocity (U) found from the flume experiments to predictions from published non-wave-based velocity equations for high-gradient channels as well as wave-based dispersion relationships (Figure 9a). The non-wave-based empirical equations were take form Yochum et al. (2012) who compared published velocity prediction methods (Jarrett, 1992; Rickenmann, 1994; Comiti et al., 2007; Ferguson, 2007; Comiti et al., 2009; Zimmermann, 2010) for high-gradient channels. We observed considerable scatter in these comparisons, with many predictions deviating substantially from the 1:1 line. We observed that predictions based on the wave dispersion formulations of White et al. (2026) ($c_d \; and \; c_g$) cluster most closely about the 1:1 line for mean velocity (Figure 9a). Among the non-wave-based methods, Ferguson (2007) performed the best for the mean velocity comparison.

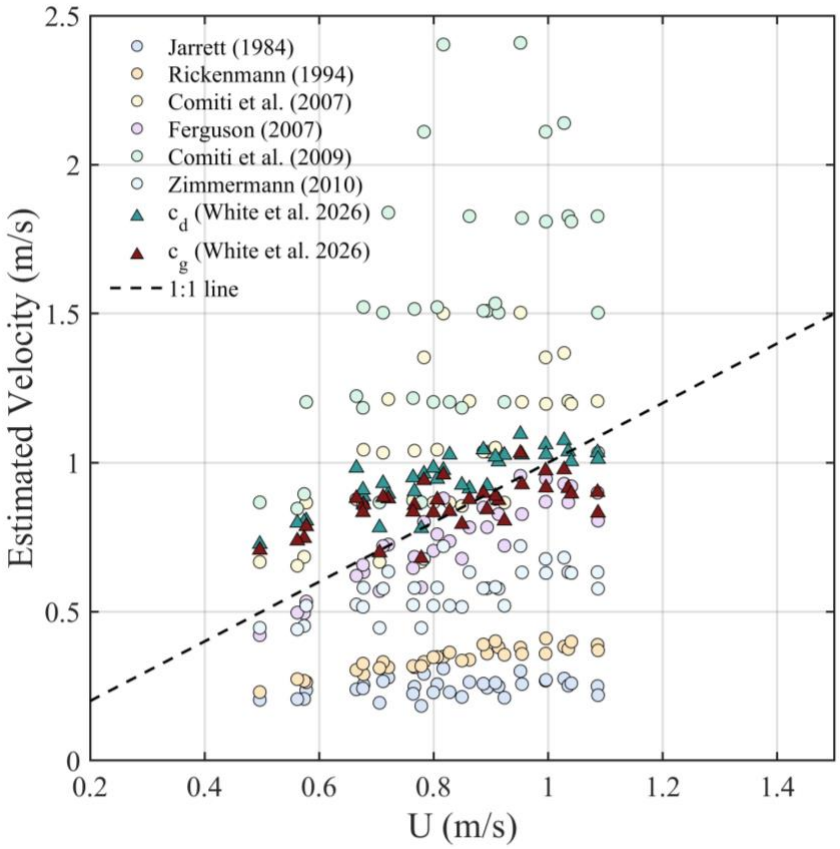

Figure 9. Comparison of predicted velocities from published non-wave-based equations and wave-based dispersion relationships with measured flume mean velocity (U).

We also compared only wave celerity estimates directly to the measured mean flow velocity and surface velocity (Figure 10a and Figure 10b). Intermediate-depth dispersion relations closely corresponded with both mean and surface velocities, whereas the deep-water dispersion relation provided a slightly better estimate for surface velocity. In contrast, shallow-water approximations systematically overpredicts both mean and surface velocities, indicating that shallow-water assumptions are not appropriate for the observed stationary wave conditions.

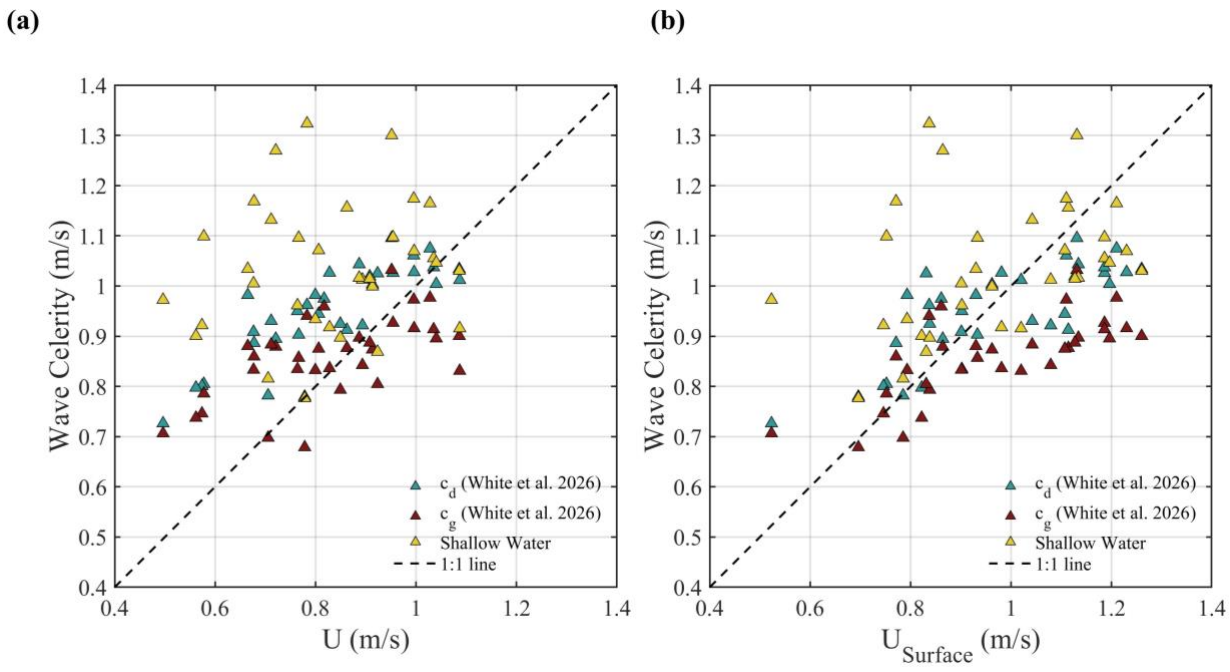

Figure 10. Comparison of wave celerity estimates derived from shallow, intermediate, and deep-water dispersion relations with (a) measured mean velocity (U) and (b) measured surface velocity ($U_{Surface}$) for stationary wave trains observed in the flume.

These results demonstrate that wave properties provide a useful proxy for flow velocity under the conditions in which stationary wave trains occur. Across the observed range of slope and discharges, we observed that the intermediate-depth dispersion relations show closer agreement with measured velocities, outperforming shallow-water approximations and supporting the use for velocity estimation in steep, high-gradient channels.

3.3 Field Observation

On a reach of the Cache la Poudre River at Canyon Mouth, Colorado, which features plane-bed, gravel-bed geomorphology (Buffington & Montgomery, 2022), stationary wave trains persisted over longitudinal distances exceeding 10 channel widths. Visual analysis of remotely sensed imagery identified four distinct stationary wave fields with measured longitudinal extents of 15.2, 24.6, 26.8, and 31.2 channel widths. We identified these four wave-train observations

using Google Earth imagery combined with high-resolution LiDAR data. We observed stationary wave trains for slopes up to 2.3% on the Poudre River (White et al., 2025).

4. DISCUSSION

4.1 Hydraulic Regime of Stationary Wave Trains

Stationary wave trains are commonly interpreted as indicators of near-critical flow (Fr ≈ 1), particularly within the framework of UHJs and critical-flow theory (Grant, 1997; Tinkler, 1997a). However, Froude numbers measured in these flume experiments indicate that persistent stationary wave trains occur across a broader hydraulic range, spanning subcritical to near-critical conditions depending on slope. At slopes ≥ 3–3.5%, reach-averaged Froude number clustered near unity, whereas at slopes of 1–2.5%, stationary waves trains occurred under subcritical conditions. These lower slopes are commonly associated with plane-bed channels (Buffington & Montgomery, 2022), where similar surface features may occur. The presence of free-surface undulations therefore does not directly imply critical flow. Chanson (1998) emphasized that undular flow may occur under near-critical conditions across a range of Froude numbers and that the existence of standing waves does not require $\mathrm{Fr} = 1$. In steep channels, local hydraulic adjustments induced by boundary roughness may therefore sustain stationary surface waves independently of strict reach-averaged hydraulic control.

All stationary wave trains in these experiments formed under very low relative submergence conditions. Akutina et al. (2019) define very low submergence as $\mathrm{h/k} < 3$, where *k* is the bed roughness height, and notes that such regimes are typically excluded from classical resistance formulations based on the logarithmic law, which assume standard submergence ($\mathrm{h/k} \approx 10 - 30$). Under very low submergence, bed roughness occupies a large portion of the flow depth, causing flow separation and wake interactions that generate vorticity at the bed and extend upward throughout the water column. These vertically structured turbulent motions

modify the velocity distribution and pressure field, introducing non-hydrostatic effects that can influence the free surface and contribute to the development of stationary wave trains. In high-gradient channels, relative bedform submergence has been shown to strongly influence flow resistance and velocity scaling (Yochum et al., 2012). Under these conditions, the shallow-water assumptions underlying the classical Froude number, hydrostatic pressure and vertically uniform velocity, are likely violated (Henderson, 1966).

In all experiments, Shields stress increased with slope, yet the bed remained immobile across all slope-discharge combinations. This confirms that the observed stationary wave trains developed independent of sediment transport or morphodynamic adjustments. Similar hydraulic behavior has been described in steep gravel-bed channels, where bed irregularities can induce hydraulic jumps and associated energy losses even as the system adjusts morphologically (Grant, 1997). The persistence of stationary wave trains under immobile-bed conditions indicates that flow alone is sufficient to sustain organized wave structure, and that neither sediment transport or bedform development is required for the formations or maintenance. Tinkler (1997a) also documented undular flows in a river with an immobile bed.

Relative depth decreased systematically with slope, placing all stationary wave trains within the intermediate-depth wave regime, where wave celerity depends on both wavelength and flow depth. This result provides a physical justification for applying the intermediate-depth dispersion relationship rather than the shallow-water or deep-water approximating when estimating mean flow velocity. The agreement between measured mean velocity in the flume and velocity predicted by the intermediate-depth dispersion equation indicates that wavelength and flow depth together can provide a reliable estimate of mean flow velocity.

4.2 Wave Nonlinearity

Wave nonlinearity increases systematically with channel slope as wave amplitude becomes larger relative to flow depth. In linear wave theory, ε is assumed to be small so that nonlinear terms in the free-surface boundary equations can be neglected. When $\varepsilon << 1$, waves fall within a weakly nonlinear regime, where nonlinear effects primarily influence wave shape while linear theory still provides a good first-order approximation of wave celerity (National Research Council, 1999). Across all experiments, ε remains below 0.2, indicating that the waves remain within the weakly nonlinear regime. Within this range, nonlinear effects influence wave shape and peak-trough asymmetry, but the linear dispersion relationship provides a first-order approximation of wave celerity (Peregrine, 1967; Mei, 1989; Dean & Dalrymple, 2002). This distinction is central to the velocity estimation approach used in this study. The wave-based methods rely on dispersion relationships derived from linear theory to relate wavelength and depth to wave celerity. If ε were large, nonlinear corrections to phase speed would be expected, potentially biasing velocity estimates derived from linear dispersion. However, the relatively small ε values observed here suggest that the waves remain within a regime where linear-based formulations should remain applicable.

Comparison of measured mean velocity to wave celerity estimated using intermediate-depth dispersion (c_g) reveals no systematic deterioration in performance with increasing ε (Figure 11). Values of U/c_g remain scattered around unity across the range of ε, and no consistent trend between ε and deviation from unity emerges. The absence of systematic deviation indicates that increasing slope, and the associated increase in ε, does not degrade the applicability of intermediate-depth dispersion within the parameter space tested. These results suggest that, within the small-amplitude regime examined here, weak nonlinearity does not exert

a dominant control on the accuracy of wave-based velocity estimation. The wave trains observed in these flume experiments therefore remains sufficiently small in ε that linear dispersion provides a robust description of wave celerity.

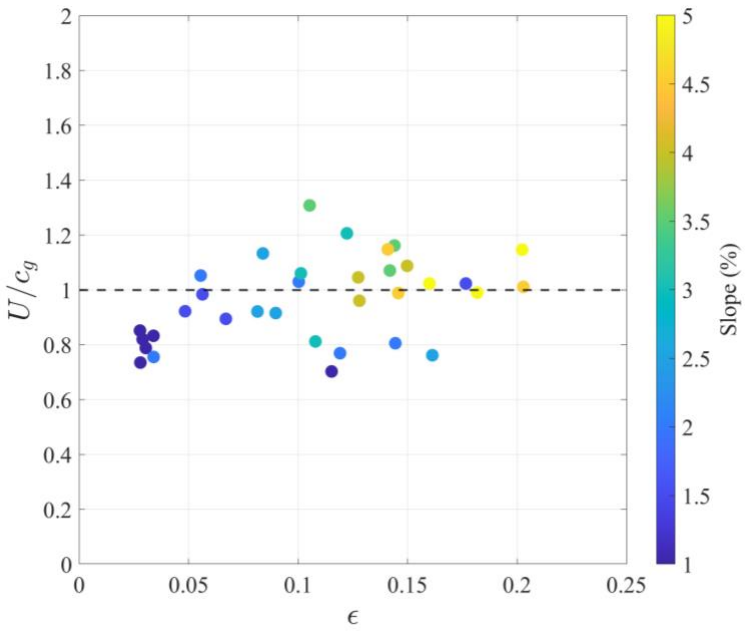

Figure 11. Relationship between wave nonlinearity (ε = a/h) and the ratio of measured mean velocity to intermediate-depth wave celerity (U/c_g).

The ratio of measured mean surface velocity to wave celerity, c_g, shows a close clustering near unity across the full range of ε, although, c_g, is less than $U_{surface}$ for nearly all observations (Figure 12). White et al. (2026) found that wave celerity estimated using c_g closely matched measured surface velocity; however, this comparison relied on detailed velocity measurements from a single smooth-bed flume experiment reported by Hu et al. (2023). In contrast, the present study evaluates the relationship between wave celerity and surface velocity across 34 flume

experiments conducted over a rough bed and similarly finds that c_g provides a close approximation of measured surface velocity, with a consistent slight underprediction.

The observation that $U_{surface} > c_g$ across the majority of the dataset (Figure 12) suggests that there are hydraulic processes that are influencing surface velocity such as bed roughness. Rough bed conditions may contribute to the systematic underprediction of surface velocity by influencing wave energy dissipation and wave propagation. Increased bed roughness enhances flow resistance and turbulence, which can dissipate wave energy and modify free-surface wave characteristics such as wavelength and amplitude. Turbulence and pressure fluctuations associated with rough beds are also known to generate gravity-capillary waves at the free surface (Dolcetti et al., 2022). In undular flows, the interaction between free-surface waves and the bed produces strong spatial variations in boundary shear stress, indicating a direct coupling between the bed and the surface wave field (Chanson, 2000). Changes in wave height and wavelength associated with increased turbulence and energy dissipation may therefore alter the wave celerity predicted by c_g. Additionally, gravity–capillary waves propagate relative to the underlying current with their own intrinsic celerity, such that the observed motion of surface features reflects a combination of wave propagation and mean flow velocity (Dolcetti et al., 2022, 2026). As a result, surface velocities measured over a rough bed may exceed celerity estimates derived solely from dispersion relationships based on flow depth, providing a potential explanation for the consistent underprediction of c_g observed in this study. The surface velocity measurements obtained from LSPIV are consistent with the theoretical interpretation presented by Dolcetti et al. (2022), which indicates that wave celerity (c_g) should approximate the depth-averaged flow velocity. Because surface velocity is typically greater than the mean velocity in open-channel flows, c_g is therefore expected to underpredict the measured surface velocity. Further

investigation into how bed roughness influences wave properties, such as wavelength and celerity, would help clarify the relationship between wave-derived velocities and surface velocity measurements.

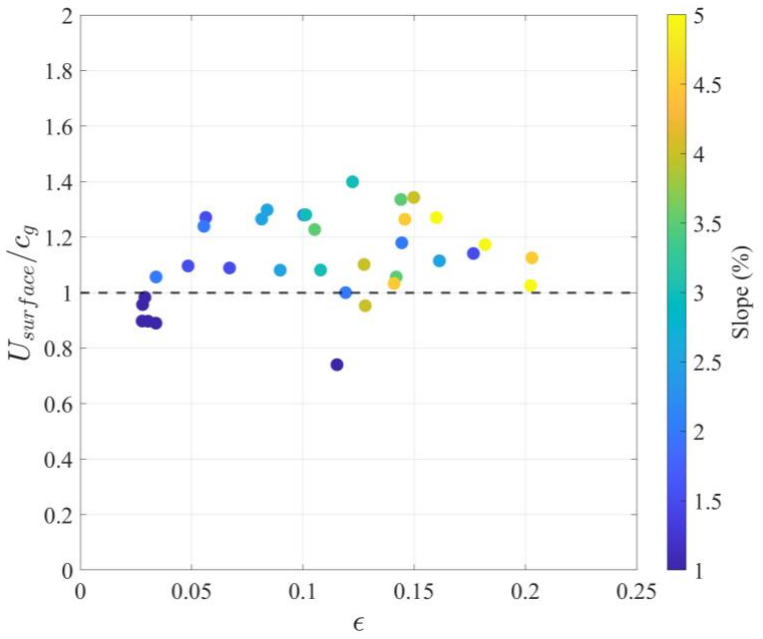

Figure 12. Relationship between wave nonlinearity (ε = a/h) and the ratio of measured mean surface velocity to intermediate-depth wave celerity ($U_{surface}/c_g$).

4.3 Velocity and Wave Celerity

Comparisons between measured velocities and wave-based velocity estimates show that dispersion relationships derived for intermediate-depth waves provide the most accurate estimates of mean flow velocity (RMSE = 0.127 m/s). In contrast, the deep-water dispersion relationship performs slightly better for estimating surface velocity (RMSE = 0.123 m/s and RMSE = 0.173 m/s respectively). The strong performance of the intermediate-depth dispersion relationship for mean velocity estimation is consistent with the observed h/L scaling, which places all stationary wave trains within the intermediate-depth regime where wave celerity depends on both depth and wavelength. The slight improvement of the deep-water dispersion

relationship for surface velocity estimation suggests that surface flow responds more strongly to wavelength scaling than to depth-dependent corrections. Recent work by White et al. (2026) similarly evaluated estimating discharge using the intermediate-depth and deep-water dispersion relationships in the context of UHJs. Together, these findings support the fundamental assumption underlying wave-based velocity estimation in stationary wave trains that wave celerity provides a reasonable approximation of mean flow velocity ($U \approx c$) when the appropriate dispersion relationship is applied.

In contrast, non-wave-based velocity prediction equations show greater scatter and inconsistent bias relative to measured velocities. Among these methods, however, the formulation of Ferguson (2007) performs best for mean velocity estimation in the present dataset (RMSE = 0.112 m/s). This result differs from Yochum et al. (2012), who reported that the Zimmermann (2010) velocity equation performed most accurately across 15 mountain stream reaches containing large wood, but overall the velocity prediction techniques based on grain size performed poorly and rather standard deviation of bed elevations improved the predictions for Yochum et al. (2012). Although the discrepancy of best performing empirical equation highlights the sensitivity of empirical resistance-based velocity predictors to channel morphology, roughness configuration, and flow resistance mechanisms.

4.4 Implications for Natural Rivers

The stationary wave trains documented here share morphological similarities with UHJs, particularly at steeper slopes, in that both exhibit undular peaks and troughs in a series of surface undulation. However, the experimental configuration and observed flow structure indicate that these wave fields are not classical UHJs. Unlike UHJs, which require a distinct supercritical-to-subcritical transition and a hydraulically defined jump toe, the stationary wave trains observed in

this study formed under quasi-uniform flow conditions without imposed tailwater control or a discrete hydraulic regime transition. These findings suggest that stationary wave trains should not be conflated with UHJs based solely on surface appearance. Mean flow depth in stationary wave trains remains approximately constant along the length of the channel. Because discharge and channel width are fixed, continuity implies that the mean velocity also remains approximately constant, and therefore the average Froude number does not vary substantially along the flume. Rather than representing a localized supercritical–subcritical adjustment, stationary wave trains emerge as spatially persistent surface gravity waves occurring under subcritical or near-critical flow conditions depending on bed slope.

Field observations indicate that undular and stationary wave features frequently coexist within rapids and substantially over short spatial scales (Magirl et al., 2009; Venditti, 2025). UHJs and stationary wave trains therefore should not be treated as mutually exclusive categories, but instead as part of a continuum of free-surface responses to steep, spatially variable flow conditions.

This interpretation parallels recent efforts in the Fraser Canyon to classify wave features based on observable surface texture properties (Ross et al., 2025). While such visually descriptive approaches provide useful geomorphic context, they emphasize surface morphology rather than underlying hydraulic structure. As discussed by Venditti (2025), rapids are often recognized by the flow structures they produce, yet they are more formally defined by the channel morphologies that generate those flow structures. Whitewater and breaking waves commonly occur where cross-sectional area is reduced, but the presence of aerated flow alone is not sufficient to define a rapid. Although supercritical flow has been argued to characterize rapid hydraulics (Kieffer, 1985, 1987, 1989; Miller, 1994), observed Froude numbers within rapids

may remain subcritical (Magirl et al., 2009; Wright et al., 2022). Accordingly, classification of stationary wave trains should consider hydraulic criteria such as relative depth, wave nonlinearity, and flow regime in addition to surface appearance.

Within this framework, stationary wave trains do not require reach-scale hydraulic control. Instead, they may emerge wherever local combinations of discharge, slope, and grain size permit surface gravity wave instabilities to persist over extended distances. Field observations of stationary wave trains in natural channels with slopes up to 2.3% have been documented using remote sensing (White et al., 2025), and such features likely occur in steeper channels associated with plane-bed morphology (Buffington & Montgomery, 2022). However, natural rivers introduce additional complexity beyond controlled laboratory conditions, including variable channel width, roughness heterogeneity, bed mobility, and unsteady discharge. Recent field-based studies demonstrate that wave persistence and spatial extent vary strongly with discharge and relative submergence, even within a single reach (Hurson, 2024; Venditti, 2025). Overall, these findings indicate that stationary waves trains arise from local flow bed interactions emphasizing the role of channel slope, grain size, and discharge rather than scale reach hydraulic control.

4.5 Limitations

The results we present here are derived from experiments conducted in a single flume configuration with fixed grain size and relatively narrow channel width and should therefore be interpreted within these constraints. The flume geometry imposed lower width-to-depth ratios than those typical of most natural rivers (Figure 6d), and the bed remained immobile throughout all experiments. While this controlled configuration was appropriate for isolating the hydraulic behavior of stationary wave trains, natural rivers exhibit variability in grain size, channel

geometry, and bed mobility that may influence the persistence, spatial extent, and scaling of these wave fields.

In steep natural channels, small variations in bed slope, roughness, or channel geometry can act as localized hydraulic controls that interrupt quasi-uniform flow and limit the downstream persistence of stationary wave trains. Field studies in large bedrock canyons, including the Fraser River, document rapids composed of spatially complex wave fields in which stationary and breaking waves coexist and reorganize with changing discharge (Magirl et al., 2009; Hurson, 2024; Venditti, 2025). These observations indicate that stationary wave trains may develop over limited portions of a reach and diminish or reorganize at higher flows, particularly where relative submergence decreases or where localized supercritical patches become more dominant.

In contrast, plane-bed reaches common in steep rivers may support laterally continuous stationary wave trains extending many channel widths under appropriate hydraulic conditions (White et al., 2025). However, channel width remains an important limitation of the present experiments. Because most natural rivers exhibit larger width-to-depth ratios, wave fields may develop with greater lateral coherence than those observed in the flume.

Despite these limitations, the controlled experiments provide a valuable hydraulic baseline. By isolating the effects of slope and discharge under fixed-bed conditions, this study establishes a reference framework that complements emerging field-based analyses. Taken together with recent observations from large rivers and bedrock canyons, the results suggest that stationary wave trains are persistent yet spatially variable features of steep channels, governed by local hydraulic balance rather than a singular flow regime. Future work should explicitly examine the

influence of channel width, bed mobility, and planform variability on the persistence and diagnostic value of stationary wave trains in natural rivers.

5. CONCLUSIONS

In this study we investigated stationary wave trains as a hydraulically definable class of surface gravity waves characterized by consistent wavelength across multiple downstream undulations and a mean water surface parallel to the bed slope. Controlled flume experiments were conducted to evaluate the hydraulic conditions under which these waves form and to test the applicability of wave-based velocity estimation methods.

We observed stationary wave trains across a range of slopes and discharges, forming under both subcritical and near-critical flow regimes depending on slope. As slope and discharge increased, waves developed under conditions approaching critical flow, accompanied by increasing wave nonlinearity. However, despite this increase in nonlinearity, intermediate-depth dispersion relationships provided the most accurate estimates of mean flow velocity among the linear wave theory formulations tested. These results demonstrate that wave-based velocity estimation using only wavelength and mean flow depth can remain accurate across varying slopes and discharges, even as wave steepness increases.

Our findings further indicate that stationary wave trains may occur independently of classical UHJs and should not be interpreted solely as indicators of critical flow. Instead, they represent organized surface gravity waves that can persist within subcritical to near-critical regimes in steep, rough-bed channels depending on slope. The flume experiments establish a controlled hydraulic framework for understanding the formation and velocity estimation for stationary wave trains.

6. REFERENCES

Airy, G. B. (1845). *Tides and Waves* (Vol. 5). Encyclopedia Metropolitana. https://books.google.com/books/about/Tides_and_Waves.html?id=LUdInQEACAAJ

Akutina, Y., Eiff, O., Moulin, F. Y., & Rouzes, M. (2019). Lateral bed-roughness variation in shallow open-channel flow with very low submergence. *Environmental Fluid Mechanics*, *19*(5), 1339–1361. https://doi.org/10.1007/s10652-019-09678-w

Buffington, J. M., & Montgomery, D. R. (2022). Geomorphic Classification of Rivers: An Updated Review. In *Treatise on Geomorphology* (2nd ed, Vol. 6, pp. 1143–1190). Elsevier. https://doi.org/10.1016/B978-0-12-818234-5.00077-8

Castro-Orgaz, O., & Hager, W. H. (2017). *Non-Hydrostatic Free Surface Flows*. Springer International Publishing. https://doi.org/10.1007/978-3-319-47971-2

Chanson, H. (2000). Boundary shear stress measurements in undular flows: Application to standing wave bed forms. *Water Resources Research*, *36*(10), 3063–3076. https://doi.org/10.1029/2000WR900154

Chanson, H. (2009). Current knowledge in hydraulic jumps and related phenomena. A survey of experimental results. *European Journal of Mechanics - B/Fluids*, *28*(2), 191–210. https://doi.org/10.1016/j.euromechflu.2008.06.004

Chanson, H., & Montes, J. S. (1995). Characteristics of Undular Hydraulic Jumps: Experimental Apparatus and Flow Patterns. *Journal of Hydraulic Engineering*, *121*(2), 129–144. https://doi.org/10.1061/(ASCE)0733-9429(1995)121:2(129)

Chow, V. T. (1959). *Open Channel Hydraulics*. McGraw Hill Book Company Inc.

Comiti, F., Cadol, D., & Wohl, E. (2009). Flow regimes, bed morphology, and flow resistance in self-formed step-pool channels. *Water Resources Research*, *45*(4), 2008WR007259. https://doi.org/10.1029/2008WR007259

Comiti, F., & Lenzi, M. A. (2006). Dimensions of standing waves at steps in mountain rivers. *Water Resources Research*, *42*(3), 2004WR003898. https://doi.org/10.1029/2004WR003898

Comiti, F., Mao, L., Wilcox, A., Wohl, E. E., & Lenzi, M. A. (2007). Field-derived relationships for flow velocity and resistance in high-gradient streams. *Journal of Hydrology*, *340*(1–2), 48–62. https://doi.org/10.1016/j.jhydrol.2007.03.021

Dean, R. G., & Dalrymple, R. A. (2002). *Water Wave Mechanics for Engineers and Scientists*. World Scientific.

Dietterich, H. R., Grant, G. E., Fasth, B., Major, J. J., & Cashman, K. V. (2022). Can Lava Flow Like Water? Assessing Applications of Critical Flow Theory to Channelized Basaltic Lava Flows. *Journal of Geophysical Research: Earth Surface*, *127*(9), e2022JF006666. https://doi.org/10.1029/2022JF006666

Dolcetti, G., Bahmanpouri, F., & Pilbala, A. (2026). Fully non-contact discharge measurement in shallow streams via physics-based water-surface image analysis. *Hydrological Sciences Journal*, 1–14. https://doi.org/10.1080/02626667.2025.2596270

Dolcetti, G., Hortobágyi, B., Perks, M., Tait, S. J., & Dervilis, N. (2022). Using Noncontact Measurement of Water Surface Dynamics to Estimate River Discharge. *Water Resources Research*, *58*(9), e2022WR032829. https://doi.org/10.1029/2022WR032829

Ferguson, R. (2007). Flow resistance equations for gravel- and boulder-bed streams. *Water Resources Research*, *43*(5), 2006WR005422. https://doi.org/10.1029/2006WR005422

Grant, G. E. (1997). Critical flow constrains flow hydraulics in mobile-bed streams: A new hypothesis. *Water Resources Research*, *33*(2), 349–358. https://doi.org/10.1029/96WR03134

Hager, W. H., & Castro-Orgaz, O. (2019). *ON THE UNDULAR HYDRAULIC JUMP AND THE UNDULAR SURGE*. 2030–2039. https://doi.org/10.3850/38WC092019-0414

Henderson, F. M. (1966). *Open Channel Flow*. Macmillian Puplishing Co. Inc.

Hu, H., Wang, H., Pan, D., Wang, X., & Bai, R. (2023). Free-surface undulation and velocity turbulence in shallow undular hydraulic jumps. *Ocean Engineering*, *269*, 113566. https://doi.org/10.1016/j.oceaneng.2022.113566

Hurson, M. (2024). *Flow Dynamics in Bedrock Canyons*. Simon Fraser University.

Jarrett, R. D. (1992). Hydrualics of Mountain Rivers. In *Channel flow resistance: Centennial of Manning's formula* (pp. 287–298). Water Resources Publications. https://books.google.com/books?hl=en&lr=&id=CHq5XTCkyakC&oi=fnd&pg=PA287&dq=jarrett+1992+hydraulics+of+mountai+nrivers&ots=b-1iVU6pGX&sig=6Ts-V1JYpCLDOAriS3GE0k12Ooc#v=onepage&q=jarrett%201992%20hydraulics%20of%20mountai%20nrivers&f=false

Kennedy, J. F. (1963). The mechanics of dunes and antidunes in erodible-bed channels. *Journal of Fluid Mechanics*, *16*(4), 521–544. https://doi.org/10.1017/S0022112063000975

Kieffer, S. W. (1985). The 1983 Hydraulic Jump in Crystal Rapid: Implications for River-Running and Geomorphic Evolution in the Grand Canyon. *The Journal of Geology*, *93*(4), 385–406. https://doi.org/10.1086/628962

Kieffer, S. W. (1987). *The Rapids and Waves of the Colorado River, Grand Canyon, Arizona* (Open-File Report) [Open-File Report].

Kieffer, S. W. (1989). Geologic nozzles. *Reviews of Geophysics*, *27*(1), 3–38. https://doi.org/10.1029/RG027i001p00003

LeCoz, J., Jodeau, M., Hauet, A., Marchand, B., & LeBoursicaud, R. (2014). *Fudaa-LSPIV* (Version 1.10.1) [Computer software]. EDF; INRAE; DeltaCAD. https://forge.irstea.fr/projects/fudaa-lspiv/

Legleiter, C. J., Grant, G., Bae, I., Fasth, B., Yager, E., White, D. C., Hempel, L., Harlan, M. E., Leonard, C., & Dudley, R. (2025). Remote Sensing of River Discharge Based on Critical Flow Theory. *Geophysical Research Letters*, *52*(9), e2025GL114851. https://doi.org/10.1029/2025GL114851

Magirl, C. S., Gartner, J. W., Smart, G. M., & Webb, R. H. (2009). Water velocity and the nature of critical flow in large rapids on the Colorado River, Utah. *Water Resources Research*, *45*(5), 2009WR007731. https://doi.org/10.1029/2009WR007731

Mei, C. C. (1989). *The Applied Dynamics of Ocean Surface Waves* (1st ed.). World Scientific. https://books.google.com/books?id=LKCQorj3XZwC&printsec=frontcover#v=onepage&q=nonlinearity&f=false

Miller, A. J. (1994). Debris-fan constrictions and flood hydraulics in river canyons: Some implications from two-dimensional flow modelling. *Earth Surface Processes and Landforms*, *19*(8), 681–697. https://doi.org/10.1002/esp.3290190803

Montes, J. S., & Chanson, H. (1998). Characteristics of Undular Hydraulic Jumps: Experiments and Analysis. *Journal of Hydraulic Engineering*, *124*(2), 192–205. https://doi.org/10.1061/(ASCE)0733-9429(1998)124:2(192)

National Research Council. (1999). *Twenty-Second Symposium on Naval Hydrodynamics*. National Academies Press.

Peregrine, D. H. (1967). *Long waves on a beach*. *27*, 815–827. https://doi.org/10.1017/S0022112067002605

Phillips, O. M. (1977). *The Dynamics of the Upper Ocean*. Cambridge University Press.

Rickenmann, D. (1994). *An alternative equation for the mean velocity in gravel-bed rivers and mountain torrents*. *1*, 672–676.

Ross, C. B., Venditti, J. G., Carr, J. C., Kusack, K., & Wright, M. (2025, December 16). *Rapids of the Fraser Canyon*. AGU25.

Stokes, G. G. (1847). *On the theory of oscillatory waves*. *8*, 441–455.

Tinkler, K. J. (1997a). Critical flow in rockbed streams with estimated values for Manning's n. *Geomorphology*, *20*(1–2), 147–164. https://doi.org/10.1016/S0169-555X(97)00011-1

Tinkler, K. J. (1997b). Indirect Velocity Measurement from Standing Waves in Rockbed Rivers. *Journal of Hydraulic Engineering*, *123*(10), 918–921. https://doi.org/10.1061/(ASCE)0733-9429(1997)123:10(918)

Venditti, J. G. (2025). *Morphodynamics of Bedrock Rivers*. https://doi.org/10.1146/annurev-earth-040523- 023051

White, D. C., Yager, E., Grant, G. E., Leonard, C., Fasth, B., & Bae, I. (2025). *Standing Wave Fields in Steep Rivers*. AGU25.

White, D. C., Yager, E. M., Legleiter, C. J., Grant, G., Hempel, L., Leonard, C., Adler, K., Harlan, M., & Fasth, B. (2026). Estimating Discharge From Undular Hydraulic Jumps: Feasibility Assessment Based on Flume Experiments. *Water Resources Research*, *62*(3), e2025WR040997. https://doi.org/10.1029/2025WR040997

Wright, M., Venditti, J. G., Li, T., Hurson, M., Chartrand, S., Rennie, C., & Church, M. (2022). Covariation in width and depth in bedrock rivers. *Earth Surface Processes and Landforms*, *47*(6), 1570–1582. https://doi.org/10.1002/esp.5335

Yochum, S. E., Bledsoe, B. P., David, G. C. L., & Wohl, E. (2012). Velocity prediction in high-gradient channels. *Journal of Hydrology*, *424–425*, 84–98. https://doi.org/10.1016/j.jhydrol.2011.12.031

Zimmermann, A. (2010). Flow resistance in steep streams: An experimental study. *Water Resources Research*, *46*(9), 2009WR007913. https://doi.org/10.1029/2009WR007913

7. APPENDICES

7.1 Appendix A: Velocity and Celerity Estimation Statistics

Table A1: The coefficient of determination (R^2) and root mean square error (RMSE) statistical analyses for velocity estimations

Name	RMSE (m/s)	R^2
Estimated vs. Mean Velocity		
Jarrett 1984	0.600	-13.997
Rickenmann 1994	0.501	-9.458
Comiti et al 2007	0.275	-2.146
Ferguson 2007	0.112	0.477
Comiti et al. 2009	0.774	-23.958
Zimmermann 2010	0.281	-2.296
c_d (White et al. 2026)	0.153	0.018
c_g (White et al. 2026)	0.127	0.323
Celerity vs. Mean Velocity		
c_d (White et al. 2026)	0.153	0.018
c_g (White et al. 2026)	0.127	0.323
Shallow water	0.293	-2.600
Celerity vs. Surface Velocity		
c_d (White et al. 2026)	0.123	0.535
c_g (White et al. 2026)	0.173	0.079
Shallow water	0.210	-0.365